

Differences in mechanical and microstructural parameters of fracture in a refractory masonry material under monotonic and cyclic loading

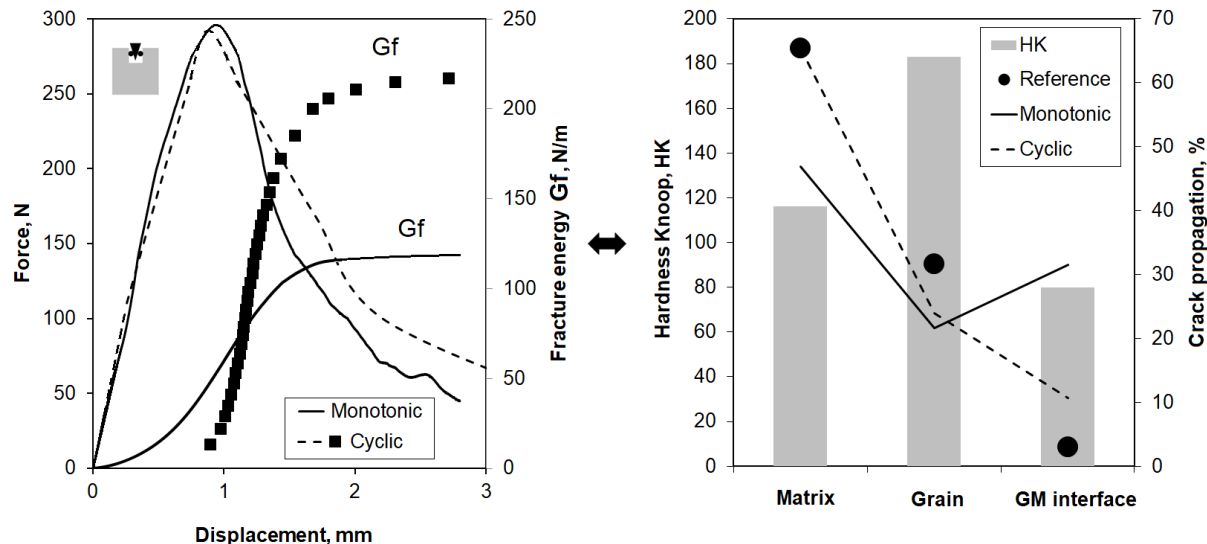
K. Andreev^{1,2}, Y. Yin², B. Luchini¹, I. Sabirov³

1 – Ceramics Research Centre, Tata Steel, 1951MD, Velsen Noord, The Netherlands

2 – The State Key Laboratory of Refractories and Metallurgy, Wuhan University of Science and Technology, 430081, Wuhan, China

3 – IMDEA Materials Institute, Getafe, 28906, Madrid, Spain

Graphical abstract



Highlights

- Knoop hardness is used to interpret the fractography and stress-strain data.
- Monotonic failure is more brittle, with same trans granular failure in both modes.
- Monotonic crack follows less energy consuming grain-matrix interface.
- Differences are due to lower energy input and matrix pre-cracking in cyclic mode.

Abstract

Refractory masonry (refractories) of industrial furnaces experience loads of various nature during service. Microstructural aspects of failure in silica refractories under monotonic and cyclic fatigue wedge splitting loading was studied. Knoop hardness measurements assisted the analysis. Monotonic and cyclic loading resulted in similar average strength with lower fracture energy for the first. With similar average crack non-linearity and trans granular failure, due to lower matrix damage and higher energy input the monotonic crack follows preferably grain-matrix interfaces (lowest energy consuming route). In cyclic mode, repeated loading increases energy dissipation. Within one loading mode, the brittleness correlates with trans granular failure.

Keywords : refractories, silica bricks, hardness, roughness, cyclic loading, wedge splitting test, fractography

1.0 Introduction

Refractory insulation materials (refractories) such as bricks and castable concrete are used to construct industrial furnaces and high temperature reactors [1]. Refractories of different chemical and mineralogical composition exist to match the variety of processes they are utilised to contain. In service, refractories experience thermal and mechanical loads of various intensity [2,3,4]. Such loads often have cyclic nature. E.g. during a typical campaign of some

40 years, refractories masonry of coke ovens experiences some 13000-15000 production cycles [5,6]. During the cycles, variation of both external force and temperature occurs. In the latter case, thermal shock conditions develop [2,7,8]. Failure of the masonry occurs either due to the single event of an irregular spike load or due to the cyclic fatigue [3,7,9].

For refractories, no specific analysis of differences between cyclic and monotonic failure has been performed so far. The design of the refractory masonry is based on either simulating thermal shock tests [5,7,8,10], stress-strain tests of either monotonic [2,7,11] or cyclic loading mode [3,7,9,12]. Under monotonic loading, higher roughness of the fracture surface is seen for materials with higher resistance to crack propagation [13]. In materials showing more brittle failure, higher percentage of trans granular cracking is observed [11]. For cyclic stress [9,12,14] and strain [3,7,12] controlled fatigue, the deterioration of interlocking in the crack tip wake and the relocation of larger grains are believed to play a critical role in the failure. The comparison of cyclic strain-controlled failure and monotonic failure in specific type of refractories featuring grains of hercynite spinel demonstrated lower fracture energy for cyclic failure [3]. Respectively, smaller fracture process zone (FPZ) was seen to develop during the cyclic loading. Contrarily to that, less brittle failure during cyclic tests was seen in silica refractories material tested in uni-axial compression and three-point bending [12]. For the latter, the difference was especially impressive, as monotonic loading tests showed abrupt failure and cyclic loading tests showed gradual strain softening. No fractographic analysis was performed to explain the phenomenon.

Due to similar microstructure of matrix consisting of smaller grains, larger grains, pores and micro-cracks, refractories have largely similar mechanical behaviour to the civil engineering concrete and rocks. For both, the concrete, and the rocks, qualitatively and quantitatively different crack propagation under monotonic and cyclic loading has been reported [15,16]. For rocks, deviations from monotonic failure trends were observed both for stress and strain ("damage") controlled cyclic fatigue of high and low amount of cycles [15]. For concrete, whether the force-displacement curves of cyclic fatigue failure exceed or fall within the envelope of monotonic loading is believed to be determined by the combined effect of loading amplitude and frequency, by the concrete's strength and its heterogeneity [16]. Generally, the cyclic failure is distinguished by higher capacity of energy absorption [17] resulting from wider FPZ with crack branching [15,17]. The failure under monotonic loading is more brittle and favours trans-granular crack propagation [15,18]. The cyclic fatigue mechanisms feature de-cohesion of the larger grains and matrix loosening [15]. Final fatigue failure involves coalescence of micro-cracks [15,16]. The same phenomenon controls the saturation of the microstructural damage during repetitive thermal-shock in technical ceramics [19].

In this work, the crack propagation under monotonic and cyclic loading was studied using samples of silica-based brick [1,5,6,7]. The microstructure related aspects of the failure were the focus of the study. Failure under the wedge splitting conditions was analysed. The cyclic tests followed strain-controlled fatigue protocols. The crack propagation was evaluated from global stress-strain parameters and by fractographic analysis. The latter quantified the crack roughness and probability of failure of different parts of the microstructure. Knoop hardness tests assessed properties of larger grains, matrix, and their interface, which allowed better correlation between the stress-strain parameters and the microstructural aspects of the crack trajectory. The results of the work are to contribute to the optimization of the material design and the material selection procedures improving the robustness of the refractories masonry structures.

2.0 Methods and materials

2.1 Materials

Commercially available silica bricks standardly used for construction of coke ovens were studied (Fig. 1). The bricks are pressed from quartzite grains using calcium hydroxide solution and sintered at temperatures of some 1500°C. The chemical and physical properties of the

material were broadly discussed elsewhere [7], where it was referred to as SB2. Typical chemical composition features 96.0 wt.% of SiO_2 , 2.5% of CaO , 1.0% of Al_2O_3 , 0.5% of Fe_2O_3 . The mineralogical composition features 63-66% of tridymite, 28-31% of cristobalite, less than 1% of quartz, 3-5% of pseudo-wollastonite. Tridymite forms the grains of the matrix and the rims of larger grains [7]. Cristobalite is predominantly found in the large grains (Fig. 1). In Fig. 1, the dark fields and lines are pores and their boundaries in the matrix, respectively. The grain size distribution as indicated by the supplier is as follows: 1-2mm grains are 2 wt.%, 0.5-1 mm are 13 wt.%, 0.1-0.5 mm are 29 wt.%, the rest is finer than 0.088mm. The bulk and true density are 1.84 g/cm^3 and 2.35 g/cm^3 , respectively. Apparent porosity is 19.6 %. The pore size distribution obtained by Hg-porosimetry shows three peaks corresponding with the pore diameters of 0.5 μm , 10 μm , $>100 \mu\text{m}$. The compressive strength at RT and at 1400 °C is 40-50 MPa and 10-15 MPa, respectively.

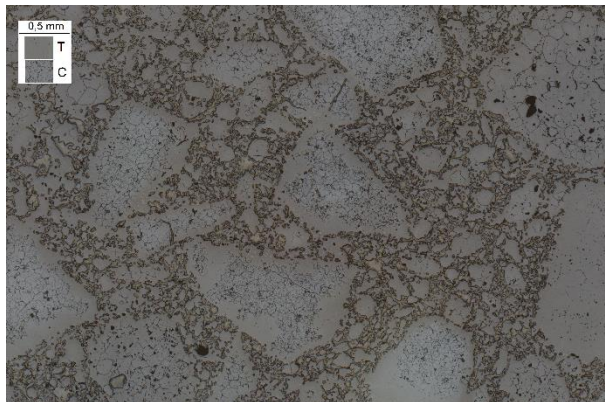


Fig. 1 Typical micro-structure of the studied material: C is cristobalite, T is tridymite.

2.2 Methods

The wedge splitting tests (WST) [20] were performed at room temperature in the test frame by Shen Zhen Wance Testing Machine Co. WST set-up was used as it allows stable crack growth and enables the development of the FPZ [21]. The test procedure and the data analysis was as in [22]. The width, depth and height of the samples were 100 mm, 65 mm and 100 mm, respectively. Due to notches, the failed cross-section had the width and height of 55 mm and 66 mm, respectively. Monotonic tests and cyclic fatigue tests were performed. Seven samples tested in each mode are numbered with a consecutive sample number for monotonic (SM) and cyclic (SC) modes. All tests were conducted with the constant vertical wedge displacement rate of 0.5 mm/min. The fatigue tests featured cycles of constant displacement (strain) amplitude. The loading protocol was as in the Method III of [12]. During the loading phase of the cycle, the amplitude stays constant. The unloading stops upon reaching the minimal force level. The next loading starts where the previous unloading stopped. Such cyclic loading protocol is seen as more representative for the in-service failure of refractories, where the loading is induced by thermal strains [12]. All cyclic fatigue tests were performed with the same amplitude, which is 90 % of the average displacement at failure (displacement at the maximal force) registered in monotonic tests. The stress-strain parameters of WST used in the analysis are notched strength (SIG-NT), fracture energy (G_f) and their ratio [22]. The ratio of $G_f/\text{SIG-NT}$ is the measure of brittleness at failure [11], the higher the ratio, the lower is the brittleness. Refractories of low brittleness are often referred to as “flexible”.

For fractographic analysis, it was aimed to select WST samples with maximal, minimal and median brittleness. After the completion of WST, the whole sample was impregnated with the epoxy resin. Due to interlocking of the cracked regions the sample was still one piece when they were impregnated by the resin. The analysis was performed on polished cross-sections cut from the sample at 25 and 50 % of the sample width, where the plain strain mode prevails. Each polished section represented the cracked part of the sample from its top to bottom. The mosaic images of the cross-sections were obtained at 5x magnification with a light optical

microscope (LOM) Zeiss Axio Imager Z1 using polarized light. On these digital images, the crack length was measured for (i) crack propagation within the matrix, (ii) crack propagation within the large grain (trans granular crack) and (iii) the crack propagation along the grain-matrix interface. The limit between the large grain and the matrix grain is considered to be 0.1 mm. The software AxioVision 4.8.3. was used. To avoid the bias during the measurement, the operator did not know the mode of failure of the analysed sample. For the reference, similar analysis was performed on random lines spanning top and bottom of the sample in the main direction of crack propagation. Two ratios characterising the crack propagation were determined. The ratio PA is the sum of lengths of cracks propagating through and along the large grain, which is divided by the total crack length L2. The ratio PBA is the ratio of length of cracks propagating through the grains divided by the sum of cracks propagating through and along the large grains. Similar analysis of the crack trajectory has been carried out for refractories [11, 22] and concrete [23]. Also, for the cracks, the total crack length (L2) and its projection on the crack direction (L1) were measured. L2 accounts for the crack branching. The ratio L2/L1 quantifies the non-linearity of the crack.

The roughness quantification was performed according to the standards ISO 11562, ISO 16610-21, ISO 4287 using the software Sigmasurf 1.0. The analysis involved the separation of the original 2D profile into waviness and roughness profiles. The spacing of points on the profile was 25 μm . The roughness parameter R_q was used. It represents the root mean square of the deviation of the profile from the mean line:

$$R_q = \sqrt{\frac{1}{l_m} \int_0^{l_m} y^2(x) dx} \quad (1)$$

Where l_m is the length of the profile, $y(x)$ is the height variation. In comparison with the most widely spread roughness parameter representing the average profile height (R_a), the parameter R_q is more sensitive to the height of occasional peaks. Due to the ambiguity of the difference between the waviness and the roughness (ISO 4287), two alternative waviness cut-off values were used. Those corresponded with the wavelength values of 8 and 2.5 mm. Also, for profiles obtained, the Fourier transform analysis was performed and the fractal Hausdorff dimension D was calculated [24].

The hardness measurements according to Knoop were performed on the same WST cross-sections as used for the fractographic analysis. The Knoop hardness of the large grains, the matrix, and the grain-matrix interface was determined. Per cross-section, between 10 and 15 indents were performed in each of the aforementioned three constituents to obtain averaged values specific for the sample. The established test and data analysis procedure was followed [25]. Tests with the load of 2 kg and the holding time of 15 sec were done. It should be noted that in a pre-study, both Vickers and Knoop tests were tried. The latter was selected for the main study as the imprint produces less auxiliary cracking upon the indentation. Also, Knoop imprints were easier to detect and to measure in the inhomogeneous microstructure of the silica bricks. Knoop tests with 1 kg and 2 kg produced statistically similar results for each category of microstructural constituents. So, the size effect was excluded in the hardness measurements. The indentation of 2 kg produced larger and easier to precisely measure imprints, especially for the matrix and grain-matrix interface.

The indentation hardness measurements are not frequently used for refractories. The information below justifies the utilization of this test in the present research. The indentation hardness is a measure of deformation resistance, which correlates with stiffness and strength [25]. For technical ceramics the indenters according to Vickers and Knoop are typically used [25]. Due to its elongated shape the Knoop indenter is believed to be most suitable for brittle ceramics. The measurement accuracy is guaranteed by utilizing sufficiently high load to avoid the size effects [25,26] and to still prevent major cracking, which reduces the apparent hardness value. [25]. Also, the indentation hardness tests are regularly used to study microstructure of civil engineering concrete, including interfacial transition zone between the aggregate grain and the paste of fine particles [27]. Some of such tests in macro, micro [28]

and nano [29] regimes are performed on polished samples impregnated with epoxy resin. For magnesia based refractories, Vickers hardness was used to assess the matrix in of different composition and after different heat treatment regimes [30].

3.0 Results

The outcomes of mechanical testing are summarized in Table 1, and typical force-displacement curves are presented in Fig. 1. The average strength is similar for SM (5.5 MPa) and SC (5.4 MPa) samples (Fig. 2, Table 1). The fracture energy calculated from the envelope of the force-displacement curves and the ratio $G_f/SIG-NT$ are in average 15-20 % higher in SC samples. The fracture energy calculated as the sum of energies consumed in all the cycles (G_f^{cyc}) is some 30-60 % higher than the envelope value. The statistical spread for the strength and the energy is rather similar in both groups. The samples of different loading modes show increasing brittleness (lower $G_f/SIG-NT$ ratio) with increasing strength (Fig. 3). The trend is more pronounced in SC. If the fracture energy is normalized by the ratio $L2/L1$ the trend becomes less significant for SC. For SM, the trend seems to disappear.

The force-displacement curves of SC have somewhat more gradual strain softening than those of SM (Fig. 2). In SC, the loading-unloading loops of individual cycles have an overlap. The loops are wide and are spread along displacement axis in the beginning and especially the end of the loading protocol. In the middle phase, the cycle loops are close to each other. Fig. 2.c compares the build-up of the cumulative energy as calculated from the envelope curve connecting the cycle peak points (G_f env cum) and from individual cycles (G_f cyc cum). The latter is the sum of energies dissipated per cycle (G_f per cyc), which are calculated from the difference between the areas under the loading and unloading branches of the given cycle. The envelope curve (G_f env cum) is similar to the energy build-up curves of SM. The cumulative energy curves have a sigmoidal shape. In the beginning phase of the test, the value of G_f cyc cum is lower than G_f env cum. However, during the middle phase significant build-up of G_f cyc cum occurs, which results in its higher final values. The final values of G_f env cum and G_f cyc cum are equal to G_f and G_f^{cyc} (Table 1), respectively.

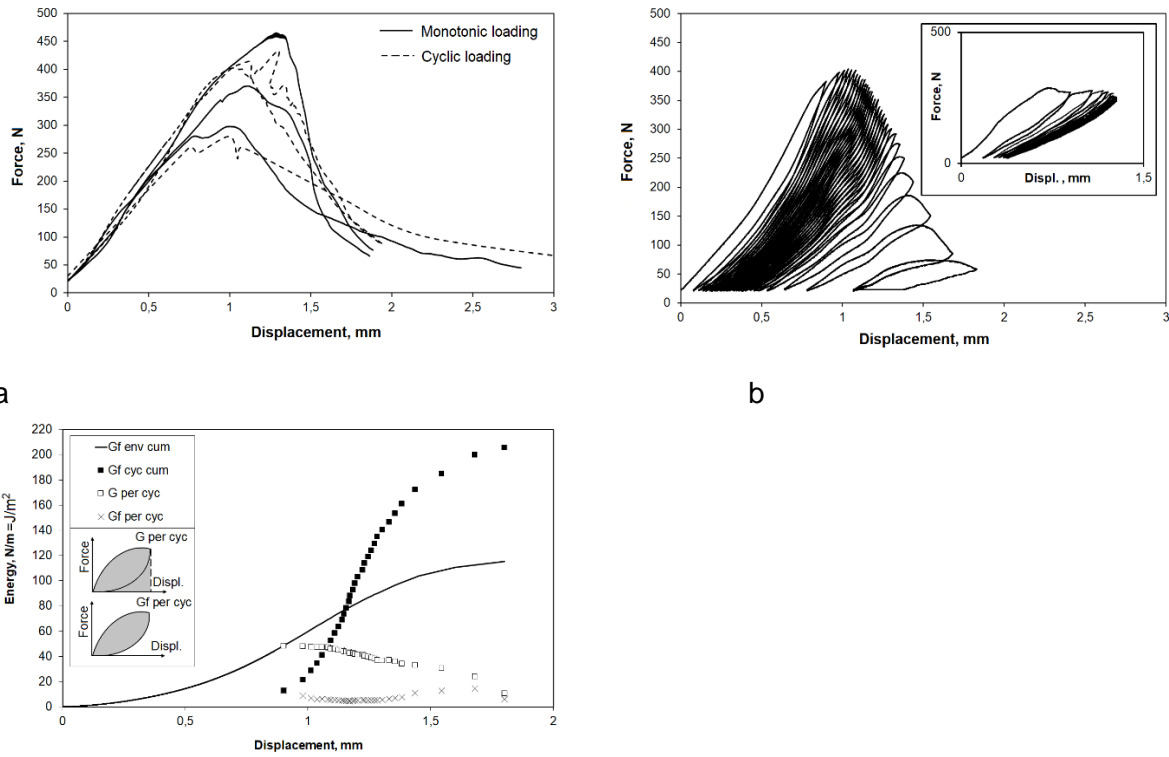
For individual cycles, the energy developed during the loading part of the cycle (G per cyc) and the dissipated energy G_f per cyc are shown (Fig. 2.c). G per cyc is calculated from the area under the loading portion of the cycle. In the beginning and middle phases of the test, the energy dissipated per cycle is much lower than the energy accumulated during the loading phase of the cycle. Only in the end of the loading program those values become close. At the same loading displacement, for all cycles after the first, G per cyc is lower than the cumulative energy G_f env cum.

Table 1

Results of WST (average for three fractography samples is in brackets).

Sample	Cycles to failure	SIG-NT, MPa	G_f , J/m ²	$G_f/SIG-NT$, mm ² /m	G_f^{cyc} , J/m ²
SM1	-	7.0	139	19.9	-
SM2	-	5.6	120	21.4	-
SM3	-	3.9	117	30.2	-
SM4	-	5.8	114	19.8	-
SM5	-	7.2	134	18.6	-
SM6	-	5.6	128	22.8	-
SM7	-	3.7	89	23.6	-
Average		5.5 (5.6)	120 (125)	22.3 (23.8)	
CV, %		24,4	13.4	17.4	
SC1	32	6.0	115	19.2	206
SC2	39	6.5	141	21.7	236
SC3	115	3.6	147	40.4	-

SC4	6	6.4	137	21.4	-
SC5	26	4.3	139	32.3	203
SC6	24	5.6	168	29.9	218
Average	40 (62)	5.4 (5.3)	143(138)	27.5(27.1)	215
CV, %	94.7	21.7	9.7	29.8	7.0
SC7	15 interrupted	3.7	-	-	-



C
Fig. 2 WST force-displacement curves, (a) curves of samples studied by fractographic analysis, (b) typical cyclic fatigue curve for SC1 and SC7 (insert), (c) energy development for the sample SC1.

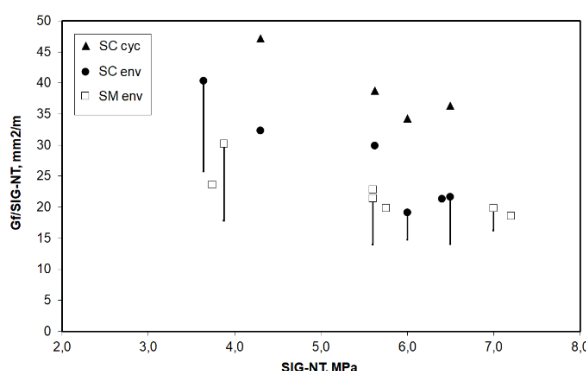


Fig. 3 Relationship between the notched strength and brittleness for individual samples. The vertical lines show the effect of the correction for L2/L1.

The fracture in the samples 1, 2 and 3 in each group was studied by fractographic analysis (Fig. 4, 5). The crack profiles show single major crack with occasional occurrences of minor crack branching. In cases when an alternative crack is branched off at higher angle, it stops quickly (e.g. SM2, SM3, Fig. 5). If the angle between the branching cracks is small, the cracks propagate for some distance almost in parallel and then re-unite (e.g. SM3, SC2). For both

loading modes, the samples with cracks of highest waviness and branching (SM3, SC3, Fig. 5) are those of lowest strength (Table 1). The sample SC3 has also the lowest for its class brittleness and needs highest number of cycles to fail. In the crack path (Fig. 4.b), there are interruptions when the crack path blends with irregularities of the microstructure. In Fig. 5 the lines with two arrowheads mark the parts of the cracks where the interruptions are frequent and where the crack between the two interruptions is not significantly longer than the interruption itself. The zones of frequent crack interruptions in the tip of the crack are typically longer in SC, where they can span some 30-40 % of the crack trajectory.

The cross-sections of the sample SC7 (Fig. 2.b insert), which was stopped after the initial 15 cycles during the middle phase of the degradation, demonstrate presence of the cracks (Fig. 6). The crack length is some 30-40 % of the cracks seen in the samples which sustained full loading program. The crack path in SC7 is frequently interrupted.



Fig. 4 Representative crack trajectory as seen for SC1, (a) the crack mouth (b) the tip of the crack.

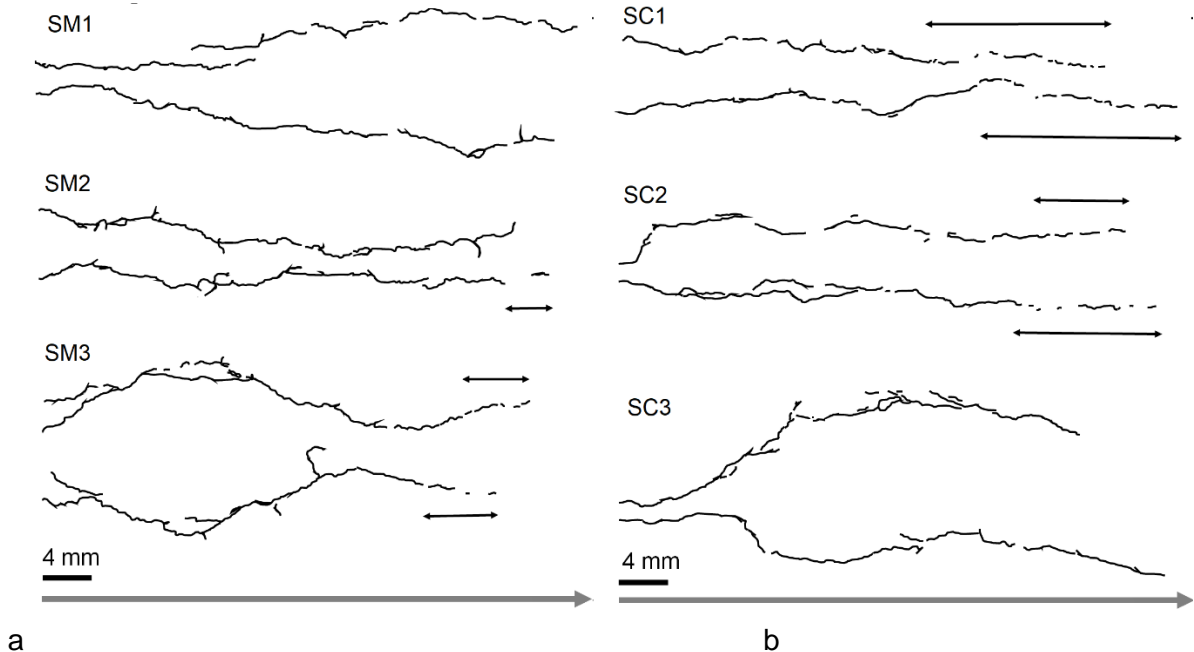


Fig. 5 Crack trajectories. The black lines with two arrowheads indicate the part of the crack featuring frequent interruptions. The grey arrow under the scale bar shows the direction of the crack propagation. Its length equals to the ligament length of the sample.

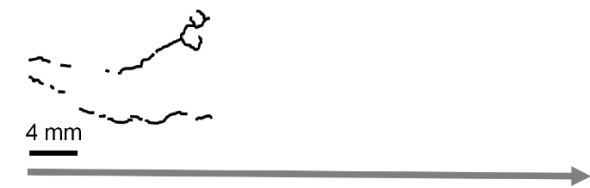


Fig. 6 Crack trajectories for SC7. The meaning of the grey arrow is as in Fig. 5.

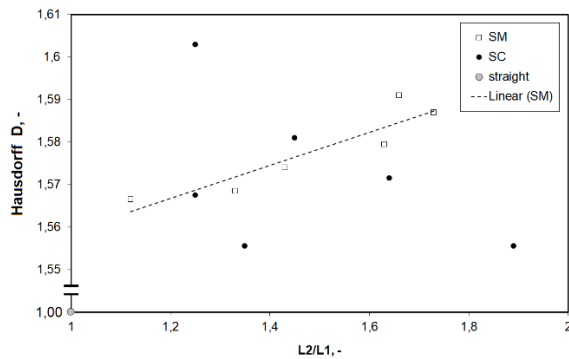


Fig. 7 Relationship between the Hausdorff constant and the ratio L2/L1.

The quantitative assessment of the crack trajectories indicates somewhat higher roughness for monotonic samples. The average R_q for the waviness cut-off of 8 mm is $171 \pm 22 \mu\text{m}$ and $164 \pm 24 \mu\text{m}$ for SM and SC, respectively. For the waviness cut-off of 2.5 mm, it is $68 \pm 5 \mu\text{m}$ and $59 \pm 6 \mu\text{m}$ for SM and SC, respectively. The average D number is 1.578 ± 0.010 and 1.572 ± 0.018 for SM and SC, respectively. The ratio L2/L1 is rather similar for SM and SC samples. The average values are 1.48 ± 0.23 and 1.47 ± 0.27 for monotonic and cyclic samples, respectively. For individual trajectories, no strong correlations between the roughness and the ratio L2/L1 was detected. The exception is the correlation between D and L2/L1 for monotonic loading (Fig. 7). However, also for that correlation its linear extrapolation to the parameters of the straight line is problematic.

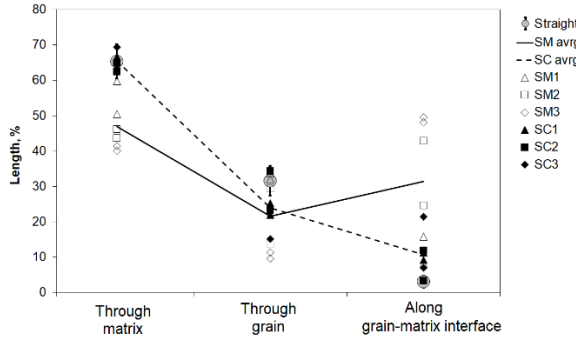


Fig. 8 Crack propagation through different constituents of the microstructure compared with the results for reference straight lines (marked as “straight”).

SM have higher portion of the crack propagating along the grain-matrix interface than it is the case with SC and in the reference straight lines (Fig. 8). Respectively, the crack portions through the grain and especially through the matrix are lower in SM. In SC, the portion of crack propagation through the matrix is as high as in the reference straight lines. The average portion for the through the grain cracking in SM, SC and in the straight lines is $21.6 \pm 11.2\%$, $23.9 \pm 6.2\%$, $31.6 \pm 4.2\%$, respectively. The average portion for the through the matrix cracking in SM, SC and in the straight lines is $46.9 \pm 7.3\%$, $65.4 \pm 2.5\%$, $65.4 \pm 4.9\%$, respectively.

The microstructural indexes of crack propagation PA and PBA have certain correlation with the roughness R_q for the cut-off of 2.5 mm and the ratio L_2/L_1 of the respective cracks. In relation to R_q , one trend is formed by PA and PBA values of different loading modes (Fig. 9). The comparison of the fractal parameter D and R_q for the cut-off of 8 mm with the parameters PA and PBA is less revealing than those of Fig. 9. The trends for L_2/L_1 are different for the SM and SC samples (Fig. 10). With growing L_2/L_1 , PA and PBA values of SM are increasing and decreasing, respectively. In case of SC, PA is apparently independent of R_q and L_2/L_1 . The ratio PBA in cyclic samples seems to follow the trend of monotonic samples. However, the sensitivity to the changing L_2/L_1 is lower (flatter trend). All the trends can be extrapolated to the parameters specific for the reference straight lines (Fig. 9, 10).

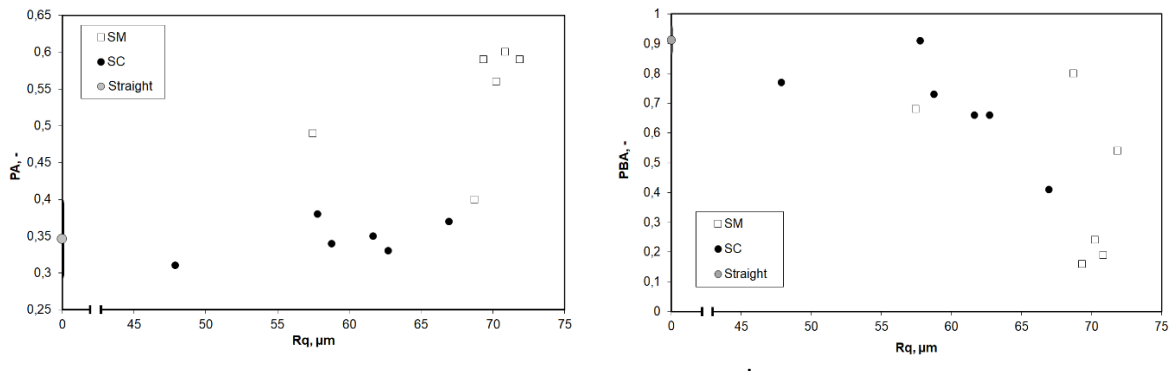
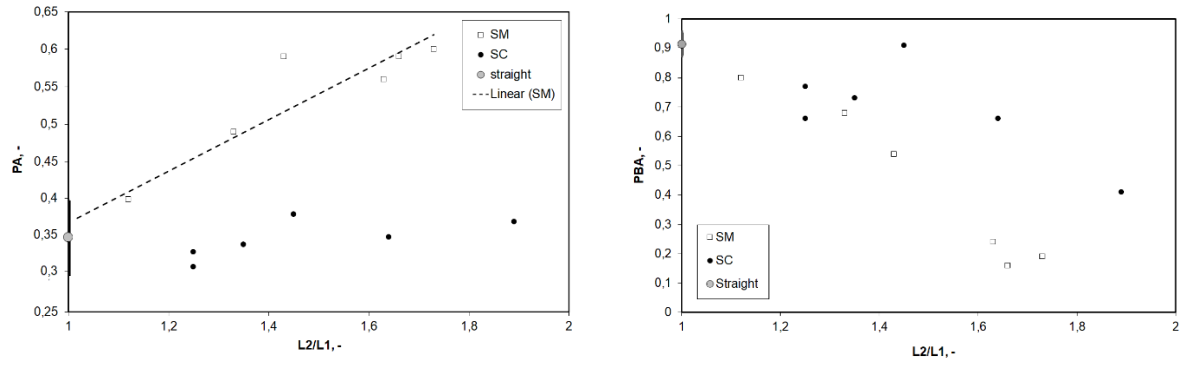


Fig. 9 Relationship between the ratios PA and PBA and the toughness R_q for the cut-off limit of 2.5 mm. “Straight” is the values for the reference straight lines.



a

b

Fig. 10 The relationship between the ratios PA and PBA and the ratio $L2/L1$. The fit in (a) is discussed in the text.

Data of only three samples with known crack propagation parameters is available per loading mode. Due to this, the attempted correlations between the stress-strain parameters and the crack trajectory specific parameters are general for both loading modes (Fig. 11). No statistically robust correlations are seen. Among the stress-strain parameters, G_f has fewer flat trends and, thus, is the most sensitive to the micro-structural parameters. G_f seems to grow with falling D , Rq and PA . G_f grows with growing PBA . Certain relationship of falling strength with growing $L2/L1$ is seen. It seems that data of monotonic tests form more obvious trends than the cyclic ones.

Among the constituents of the microstructure, the hardness was increasing in the order from interface to matrix to the large grain (Fig. 12, Table 2). The coefficient of variation for the hardness in the matrix and the interface was above 20 %. For the grain, this value was almost twice as low. The distribution of hardness in the grain followed the gradient mineralogical composition featuring higher content of tridymite and cristobalite in the rims and in the centre of the grains, respectively. The normalized hardness was obtained regarding the average hardness values of the constituents of the microstructure in the specific sample and their portion in the respective crack trajectory. In general, for both loading modes, normalized hardness shows certain trends with all the stress-strain parameters (Fig. 11.b). The positive correlation of the normalized hardness with $SIG-NT$ has a goodness of fit of 0,76. This is the only trend, among those of Fig. 11, that has the goodness of fit above 0,7. This makes it a statistically robust correlation. The hardness has positive and negative trends with the fracture energy and the brittleness ratio, respectively (Fig. 11.b). Normalised hardness has good correlation with PBA . Its correlation with $L1/L2$ is similar to that of PBA . Respectively, the correlation of normalized hardness with roughness parameters is similar to that of $L1/L2$ and PBA . Hardness of all the constituents of microstructure were significantly higher than that of the epoxy resin, used to prepare the polished section. The hardness of the epoxy resin was 5 HK.

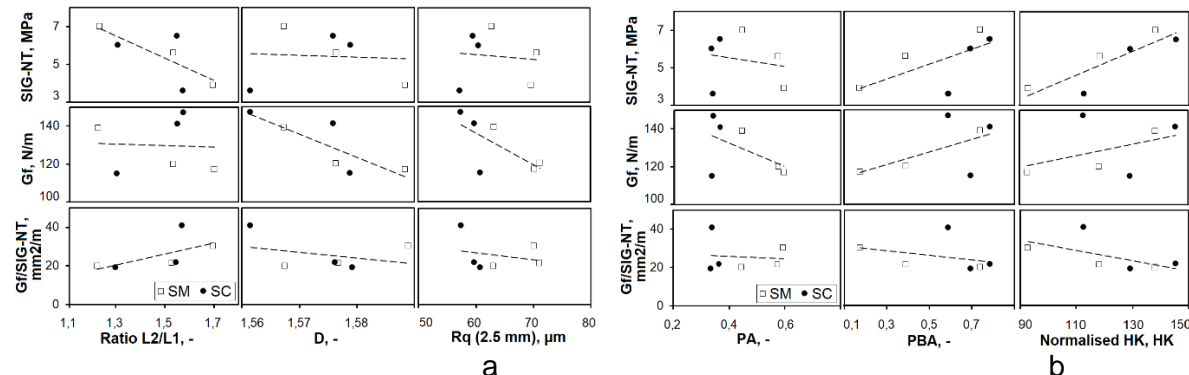


Fig. 11 Relations of the average crack trajectory parameters of a sample with its stress-strain parameters.

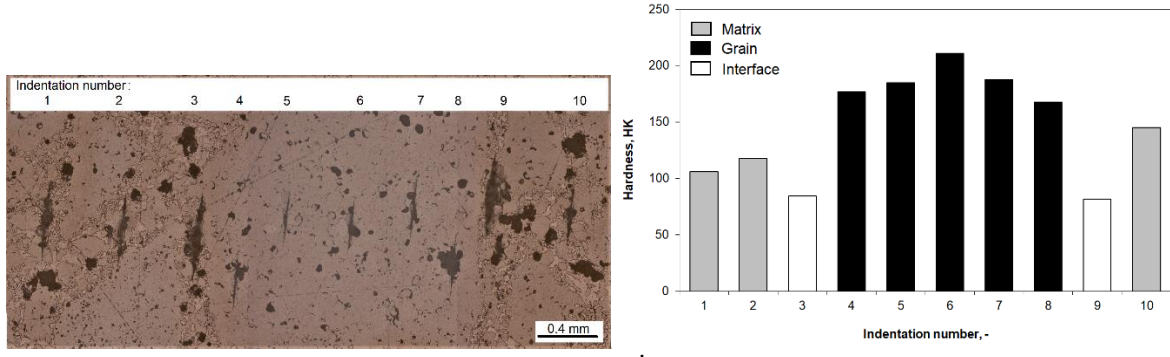


Fig. 12 Representative results of Knoop hardness tests in SC1, (a) indentation imprints in different microstructural constituents, (b) corresponding Knoop hardness values.

Table 2

Hardness data

Sample	Matrix	Grain	Interface
	HK (CV %)	HK (CV %)	HK (CV %)
SM1	118 (27)	191 (7)	86 (12)
SM2	116 (23)	183 (12)	80 (21)
SM3	107 (18)	167 (13)	65 (29)
SC1	113 (30)	194 (15)	85 (23)
SC2	131 (25)	194 (13)	84 (21)
SC3	107 (18)	167 (13)	65 (29)
SC7	120 (18)	186 (13)	92 (9)
Average	116 (23)	183 (12)	80 (21)

4.0 Discussion

In agreement with the results for other types of granular materials [15,17] and our previous research [12], the cyclic failure was found to be less brittle than the failure under monotonic loads. However, unlike in other materials, the reason of lower brittleness is neither more extensive crack branching (Fig. 4, 5), nor more tortuous crack path due to lower percentage of through the grain failure (Fig. 8). The crack non-linearity L2/L1 is similar for both modes. The lower brittleness in SC must result from longer FPZ developing in largely unbranching crack and from differences in the microstructural set-up of FPZ due to differences in the crack trajectories. For the analysis of the latter, the correlation between the microstructural aspects of failure and the global stress-strain parameters is critical.

Larger fracture process zone shows itself in SC as the zones of frequently interrupted cracks at the tips of the crack (Fig. 5). The absence of branching developing in the process zone must be due to the brittle nature of silica refractories, which results from the strong cohesion between the grains and the lack of properties mismatch between the constituents of the microstructure [7]. During the cyclic tests, friction due to repetitive opening and closing of (micro-)cracks occurring in FPZ promotes energy dissipation. Larger FPZ further intensifies this effect. Respectively, one should notice intensive growth of G cyc cum seen in the middle phase of the cyclic WST (Fig. 2.c). For cyclic fatigue tests, the middle phase of degradation is characterized by overcoming the micro-structural resistance to the crack growth, e.g. by the reduction of friction and interlocking [12,15,16,31]. Micro-damage growth and coalescence occurs in this phase. Presence of multiple non-connected cracks in the sample SC7, where the loading was stopped during the middle phase, should be the illustration of the process.

The trajectories of SM have higher roughness, especially $Rq(2,5\text{mm})$. This should result from higher portion of around the grain failure and be caused by the larger grains protruding on the fracture surface. The matrix consisting of smaller grains produces smoother cracks. This is supported by the fact that the roughness increases with higher portion of either through or around the grain fracture (higher PA) and that it decreases with higher portion of through the grain failure (higher PBA) (Fig. 9). Smaller difference between the loading modes seen for the roughness with the waviness cut-off threshold of 8mm is due to the fact that with higher cut-off both waviness of lower wavelength and the roughness is counted as roughness. As the size of larger grains is 1-2 mm, the waviness cut-off threshold of 2,5 mm seems to be more appropriate.

The trajectories of SM have higher percentage of around the grain (along the grain / matrix interface) failure and somewhat lower percentage of through the matrix failure than in SC. Respectively, FPZ of SM includes higher portions of around the grain failure. The around the grain failure is expected to promote tortuous crack path and its branching. However, the crack branching was seen to not occur. With similar $L2/L1$ ratios, higher roughness of SM could cause higher interlocking of the crack sides and the resulting resistance to the crack propagation. In the present case, the repetitive energy consumption events at less points of interlocking of SC must outweigh the energy consumption at more points of interlocking under monotonic loading. In addition, the interlocking effects due to around the grain crack propagation was not as high as expected. E.g., for monotonic tests lower roughness (Rq , D) and higher portion of around the grain failure (PBA) tend to produce higher G_f (Fig. 11). The indentation tests show that the grain matrix boundary is weaker than both matrix and the grain. This can be due to higher porosity in the interface zone and lower sintering activity of the larger grains. Probably, the energy needed to produce the new crack surfaces along the interface is rather low, which can outweigh the energy consumption due to the interlocking.

The explanation of the mechanism causing the differences in the trajectories between SM and SC is complicated by the variation of the failure parameters in samples of one loading mode. In this respect, the correlations of $L2/L1$ with the strength (Fig. 11.a), PA and PBA (Fig. 10) is interesting. Higher stress at failure typically means higher elastic energy built-up before the crack initiation. This should explain the fact that cracks in samples of higher strength have lower $L2/L1$ (Fig. 11). Such cracks deviate less from the flat crack plane (straight fracture line) (Fig. 4) and have higher portion of the through the grain failure (Fig 10.b). The cracks propagating with less energy available are possibly less sensitive to the main cracking direction and deviate towards local defects. As an example, one should see SC3 which due to the deviation of the crack sustained significantly more loading cycles than other SC samples. The fact that negative trend between the strength and the ratio of $G_f/SIG-NT$ becomes less significant if the correction for the $L2/L1$ is made (Fig. 3), indicates that the lower brittleness of lower strength samples results, to some extent, from the increased fracture surface.

The fracture process is determined by the balance between the elastic energy available at the onset of fracture and the ability of the material to dissipate it. At fracture, higher energy built-up results in faster acceleration of cracks [32]. An overview of the loading rate effects on the failure of concrete demonstrates that conflicting mechanisms may exist in the conditions of the balance between the available and the dissipated energy [33]. According to the first mechanism, higher energy input during the higher rate loading has a potential to distribute more energy in a larger zone. Also, in brittle materials, such as glass, higher ratio between available energy and the energy consumed by the crack formation is characterized by intensive crack branching and oscillation [32, 34]. Low energy crack is straight and has no branching. According to the second mechanism, the higher rate loading has lower ability of the stress relaxation at the crack tip and thus should have lower fracture process zone. Materials with lower fracture process zone are to develop more linear cracks. In our case, the cyclic loading is characterized by lower energies available to propagate the crack (G per cyc vs G env cum in Fig. 2.c). Although in Fig. 2.c G env cum is for the cyclic sample, the curve is also

representative for the monotonic loading. Also, regular unloading is to deaccelerate the crack. The relations to L2/L1 of individual samples discussed above (Fig. 10) seem to follow the second mechanism. The first mechanism could be used to explain the differences between the two loading modes. Higher potential of the monotonic loading to distribute the energy and to develop oscillating cracks may explain why monotonic cracks "find" the grain matrix interfaces, which are weaker and thus more profitable for the crack propagation. Such ability may be further promoted by the deflecting effect of the around the grain propagation of lower energy fracture. That is the overlapping effects of two mechanisms may occur, when due to the first mechanism the monotonic crack meets the grain and when due to the second mechanism it either cracks it or grows around it with subsequent deflection. In the cyclic samples, the low sensitivity of PBA to the changing L2/L1 is due to overall lower energy levels.

The preference for the through the matrix propagation under the cyclic loading can be influenced by the matrix damaging in the frontal zone of the crack. Such damaging (micro-cracks) develop according to the mechanisms specific for cyclic loading and involving occurrence of local stresses due to interlocking and irreversible displacements. Rotation of larger grains under repetitive loading and subsequent cracking of the matrix was described as the mechanism initiating the cyclic fatigue failure in carbon bonded refractories [35]. Under loading, the large grain of an irregular shape can rotate. Upon unloading, friction and debris formation does not allow the grain to return to its original position. Instead, damage occurs in the matrix to re-allocate the grain. The corners of the large grains are most probable location of the damage formation. With subsequent cycles the degradation becomes progressive and leads to the formation of micro-cracks in the matrix. The micro-cracks formed ahead of the crack tip can effectively divert the crack from the along the grain-matrix interface propagation.

Complex nature of correlations between the global material failure properties and the micro-structural parameters of the crack trajectory were noted elsewhere [11]. There, for different materials under monotonic loading there was a certain correlation of the through the grain failure with the brittleness, but not with the fracture energy. Indentation tests, and such parameters as normalized hardness, seem to be quite useful. The weakness of the interface demonstrated by Knoop hardness measurements is also supported by the fact that in SC the percentage of the around the grain and through the grain failure is, respectively, higher, and lower than in the reference lines (Fig. 8). At the same time, the percentage of the through matrix failure for SC is similar to the reference lines. That is, if a crack meets a grain, the probability of the around the grain propagation is higher than for a random reference straight line.

The correlation between the stiffness, the strength and the normalized hardness is well known for ceramic materials [25]. As the strength in both modes is similar, the correlation observed by us could be attributed to the variation of the microstructural characteristics of the samples within each mode of loading (Fig. 11.b). Representing the surface under the stress-strain curve, the value of fracture energy can be related to the hardness via strength. In the brittleness ratio, such effects are not to be expected. The presence of the trend between the brittleness ratio and the normalized hardness may indicate that hardness specific for the crack trajectory may be indicative for the energy dissipation during the crack propagation.

The evidence of different fracture behaviour under monotonic and cyclic loading has direct importance for the assessment of materials and the design of refractories masonry. Whether the cyclic failure is characterised by lower brittleness and higher fracture energy for all refractories is not clear. Regarding the complexity of the observed mechanisms and the variety of existing micro-structures in refractory masonry, the scenario when higher fracture energy failure develops during the cyclic loading seems to be possible. The analysis presented here is centered at the mechanical loads. Regarding general similarities between the cyclic mechanical and thermal shock failure seen for refractories [36], technical ceramics [36, 37] and steel [38], effects similar to those described above can be expected during thermal shock.

Conclusions

The paper presents the evidence of differences in mechanical and microstructural parameters of fracture in the masonry material of silica refractories under monotonic and cyclic loading. Within the sample groups of the monotonic and cyclic loading, the known trends of reducing crack non-linearity and increasing through the grain failure with increasing brittleness and strength are observed. These phenomena do not explain the differences between the loading modes. The monotonic loading is seen to produce more brittle failure, characterised by similar strength but lower fracture energy than the cyclic one. On microstructural level, this is seen in a supposedly less developed FPZ of largely unbranching cracks and in microstructural differences in the crack trajectories. With similar average crack waviness and through the grain failure, the monotonic crack has higher portion of the more energy efficient around the grain (along the grain-matrix interface) failure. The ability of the monotonic crack to “find” the more energy efficient route is attributed to the higher energy input during the loading process. Apart from that, the cyclic crack can be diverted from the around the grain propagation by micro-cracks formed in the matrix due to degradation mechanisms typical for the cyclic fatigue loading, e.g. large grain rotation. High energy dissipation reducing the brittleness under cyclic failure is due to the repetitive friction events during the development of FPZ. Further research is to demonstrate the applicability of the present finding to other classes of refractories and to the thermal shock induced failure.

Conflict of interest

The authors declare no conflict of interest.

Acknowledgements

Part of the work done at WUST was done within the grant National Key R&D Program of China (No. 2018YFF0214500). The authors are thankful to Tata Steel Europe for in-kind support of the work. The support of Paula Luna Dias in processing of data is gratefully acknowledged.

References

- [1] Y. Shinohara, Refractories handbook, Japanese Association of Refractories, Tokyo, 1998.
- [2] Ch. Schacht, Refractory linings: thermo-mechanical design and applications, Marcel Dekker Inc, New York, 1995.
- [3] Y. Dai, Y. Li, S. Jin, H. Harmuth, X. Xu Fracture behaviour of magnesia refractory materials under combined cyclic thermal shock and mechanical loading conditions. JAmCerSoc 2019 <https://doi.org/10.1111/jace.16856>
- [4] V. A. Perepelitsyn, F. L. Kapustin, K. G. Zemlyanoi, L. V. Ostryakov, L. P. Yakovleva, I. G. Maryasev, L. M. Mikhailovskaya, Crack genesis in refractories. Refractories and Industrial Ceramics 57-4 (2016) 394-400 DOI 10.1007/s11148-016-9991-9
- [5] T. Arahori, T. Suzuki, K. Fujisawa, Mechanical behavior of silica refractories under thermal cycle, Yogyo-Kyokai-Shi 91-11 (1985) 32-39. (In Japanese)
- [6] Andreev, K., Wijngaarden, M.V., Put, P. Tadaion V., Oerlemans O. Refractories for Coke Oven Wall – Operator’s Perspective. Berg Huettenmaenn Monatsh (2016). doi:10.1007/s00501-016-0563-6
- [7] K. Andreev, V. Tadaion, Q. Zhu, W. Wang, Y. Yin, T. Tonnesen, Thermal and mechanical cyclic tests and fracture mechanics parameters as indicators of thermal shock resistance – case study on silica refractories, Journal of the European Ceramic Society, Vol. 39-4 (2019) 1650-1659.
- [8] K. Andreev, B. Luchini, M.J. Rodrigues, J. Lino Alves, Role of fatigue in damage development of refractories under thermal shock loads of different intensity Ceramics International 46 (2020) 20707–20716
- [9] Y. Hino, Y. Kiyota, Fatigue failure behaviour of Al₂O₃–SiO₂ system bricks under compressive stress at room and high temperatures, ISIJ International, 52-6 (2012) 1045–1053.

[10] B. Cotterell, S.W. Ong, C. Qin, Thermal Shock and Size Effects in Castable Refractories. *Journal of the American Ceramic Society* 78 (1995) 2056-2064

[11] H. Harmuth, R.C. Bradt, Investigation of refractory brittleness by fracture mechanical and fractographic methods, *Interceram Refractories Manual* 1 (2010) 6-10.

[12] K. Andreev, V. Tadaion, J. Koster, E. Verstrynghe, Cyclic fatigue of silica refractories - effect of test method on failure process, *J Eur Ceram Soc* 37-4 (2017) 1811-1819.

[13] C. Manhart, H. Harmuth. Use of a stereoscopic method for the fractographic characterization of ordinary ceramic building materials. *Prakt. Metallogr.* 43-9 (2006) 438-449

[14] K. Andreev, M. Boursin, A. Laurent, E. Zinngrebe, P. Put, S. Sinnema, Compressive fatigue behaviour of refractories with carbonaceous binders, *J of Eur. Cer. Soc.* 34-2 (2014) 523-531.

[15] Cerfontaine B, Collin F. Cyclic and fatigue behaviour of rock materials: review, interpretation and research perspectives. *Rock Mech Rock Eng* 2018;51:391–414. <https://doi.org/10.1007/s00603-017-1337-5>.

[16] K. Kirupakaran, J.M. Chandra Kishen. Micromechanics of fracture and failure in concrete under monotonic and fatigue loadings. *Mechanics of materials* (2020) <https://doi.org/10.1016/j.mechmat.2020.103490>

[17] Z. Song, T. Frühwirt, H. Konietzky, Inhomogeneous mechanical behaviour of concrete subjected to monotonic and cyclic loading. *International Journal of Fatigue* 132 (2020) <https://doi.org/10.1016/j.ijfatigue.2019.105383>

[18] N. Erarslan, H. Alehossein, D.J. Williams Tensile fracture strength of brisbane tuff by static and cyclic loading tests. *Rock Mech Rock Eng* 2014;47:1135–51. <https://doi.org/10.1007/s00603-013-0469-5>.

[19] E.D. Case, The saturation of thermo-mechanical fatigue damage in brittle materials. 137-208 In. *Thermo-mechanical Fatigue and Fracture*, Edt. M.H. Aliabadi, WIT-Press, Southampton, Boston, 2002

[20] H. Harmuth, K. Rieder, M. Krobath, E. Tscheegg, Investigation of non-linear fracture behaviour of ordinary ceramic refractory materials, *Mater. Sci. Eng. A-Struct.* 214 (1) (1996) 53–61.

[21] Y. Dai, D. Gruber, H. Harmuth, Observation and quantification of the fracture process zone for two magnesia refractories with different brittleness. *Journal of the European Ceramic Society* 37 (2017) 2521-2529

[22] T. Zhu, Y. Li, S. Sang, Z. Xie, Fracture behavior of low carbon MgO–C refractories using the wedge splitting test, *J Eur Ceram Soc* (2016), <http://dx.doi.org/10.1016/j.jeurceramsoc.2016.11.013>

[23] C. Rossello, M. Elices, G.V. Guinea, Fracture of model concrete: 2. Fracture energy and characteristic length. *Cement and concrete research* 36 (2006) 1345-53

[24] M. Schroeder. Fractals, chaos, power laws. W.H. Freeman (1991) New York

[25] J. Pelleg. Mechanical properties of ceramics. Springer (2014) ISBN 978-3319044910

[26] T. Wilantewicz, W.R. Cannon, G.D. Quinn, The intendant size effect for five ceramic materials. *Ceramic Engineering and Science Proceedings* (2006) DOI: 10.1002/9780470291368.ch20

[27] A. H Asbridge; C. L Page; M. M Page Effects of metakaolin, water/binder ratio and interfacial transition zones on the microhardness of cement mortars. *Cement and Concrete Research* 32-9- (2002)1365-1369 DOI: 10.1016/S0008-8846(02)00798-6

[28] S. Taheri , G. Pareja Delgado, O.B.A. Agbaje, P. Giri, S.M. Clark Corrosion Inhibitory Effects of Mullite in Concrete Exposed to Sulfuric Acid Attack. *Corros. Mater. Degrad.* 2020, 1, 282–295; doi:10.3390/cmd1020014

[29] Hankun Liu, Xiaodan Ren, Shixue Liang, Jie Li Physical Mechanism of Concrete Damage under Compression Materials 2019, 12, 3295; doi:10.3390/ma12203295

[30] C. Gómez-Rodríguez, G.A. Castillo-Rodríguez, E.A. Rodríguez-Castellanos, F.J. Vázquez-Rodríguez, J.F. López-Perales, J.A. Aguilar-Martínez, D. Fernández-González, L.V. García-Quiñonez, T.K. Das-Roy, L.F. Verdeja, Development of an ultra-low carbon MgO refractory doped with α -Al₂O₃ nano-particles for the steelmaking Industry: a

microstructural and thermo-mechanical study. Materials 13 (2020) 715; doi:10.3390/ma13030715

[31] F. Thummen, C. Olagnon, N. Godin, Cyclic fatigue and lifetime of a concrete refractory. J Eur Ceram Soc. 26 (2006) 3357–63.

[32] Karma, A.E. Lobkovsky, Unsteady crack motion and branching in a phase-field model of brittle fracture. Physical review letters 92-24 (2004) DOI: [10.1103/PhysRevLett.92.245510](https://doi.org/10.1103/PhysRevLett.92.245510)

[33] Z.P. Bazant, R. Gettu, Rate effects and load relaxation in static fracture of concrete. ACI materials journal 9-10 (1992) 456-468

[34] G.D. Quinn Fractography of ceramics and glasses. NIST Special Report (2016) <http://dx.doi.org/10.6028/NIST.SP.960-16e2>

[35] K. Andreev, M. Boursin, A. Laurent, E. Zinngrebe, P. Put, S. Sinnema, Compressive fatigue behaviour of refractories with carbonaceous binders, J of Eur. Cer. Soc. 34-2 (2014) 523-531.

[36] P.K. Panda, T.S. Kannan, J. Dubois, C. Olagnon, G. Fantozzi, Thermal shock and thermal fatigue study of alumina. J. Eur. Cer. Soc. 22 (2002) 2187-2196

[37] B.A. Wilson, E.D. Case. Comparison of mechanical fatigue with thermal fatigue in ceramics. Scripta Metallurgica et materialia. 28 (1993) 1571-1576

[38] A. Fissolo, C. Robertson, V. Maillot, Prediction of crack initiation and growth in thermal fatigue 68-105 In. Thermo-mechanical Fatigue and Fracture, Edt. M.H. Aliabadi, WIT-Press, Southampton, Boston, 2002